ACS APPLIED MATERIALS & INTERFACES

RESEARCH ARTICLE

www.acsami.org

Control of Interface Nanoscale Structure Created by Plasma-Enhanced Chemical Vapor Deposition

Someswara R. Peri,[†] Bulent Akgun,[‡,§] Sushil K. Satija,[‡] Hao Jiang,[⊥] Jesse Enlow,[⊥] Timothy J. Bunning,[⊥] and Mark D. Foster[†,*]

[†]Institute of Polymer Science and Polymer Engineering, The University of Akron, 170 University Avenue, Akron, Ohio 44325-3909, United States

[‡]NIST Center for Neutron Research, Gaithersburg, Maryland 20899, United States

[§]Department of Materials Science and Engineering, University of Maryland, College Park, Maryland 20742, United States

[⊥]Air Force Research Laboratory, Materials and Manufacturing Directorate, Wright-Patterson Air Force Base, Ohio 45433, United States

Supporting Information

ABSTRACT: Tailoring the structure of films deposited by plasma-enhanced chemical vapor deposition (PECVD) to specific applications requires a depth-resolved understanding of how the interface structures in such films are impacted by variations in deposition parameters such as feed position and plasma power. Analysis of complementary X-ray and neutron reflectivity (XR, NR) data provide a rich picture of changes in structure with feed position and plasma power, with those changes resolved on the nanoscale. For plasma-polymerized octafluorocyclobutane (PP-OFCB) films, a region of distinct chemical composition and lower cross-link density is found at the substrate interface for the range of processing conditions studied and a surface layer of lower cross-link density also appears when plasma power exceeds 40 W. Varying the distance of the feed from the plasma impacts the degree of cross-linking in the film center, thickness of the surface layer, and thickness of the transition region at the substrate. Deposition at the highest power, 65 W, both enhances cross-linking and creates loose fragments with fluorine content higher than the average. The thickness of the low cross-link density region at the air interface plays an important role in determining the width of the interface built with a layer subsequently deposited atop the first.

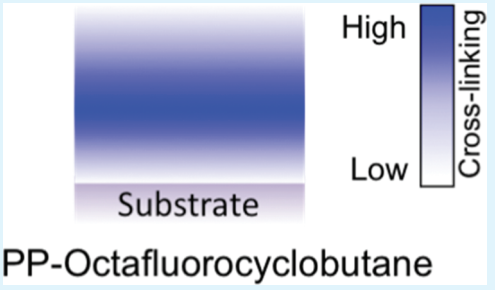

KEYWORDS: cross-link density, plasma polymerization, PECVD process parameters, PECVD interfaces, vapor-swelling, X-ray/neutron reflectivity

1. INTRODUCTION

Plasma polymerized homopolymer films, such as that shown schematically in Figure 1, have great potential for use in a wide range of applications, including optical devices such as sensors and filters and biofilms for protecting implants.[1−4] PECVD can be used to create pinhole-free films having a robust, cross-linked structure, and good adhesion to a variety of substrates.[5−8] The interfaces formed differ in two ways from the polymer interfaces most widely studied. First, the material at the interface is cross-linked. Secondly, because the polymer is created by the deposition, the deposition process plays a larger role in dictating the interfacial structure. Kim et al.[9] found plasma polymerized (PP) homopolymer films from deuterated-benzene (dB) and octafluorocyclobutane (OFCB) precursors processed under one particular set of conditions had extremely smooth film/air interfaces and uniform structure through the depth of the film except for a very thin (≈ 1 nm) transition layer next to the substrate for films made from OFCB. They argued that the structure resulting from the deposition of reactive fragments on an oxide differs from the structure deposited on previously formed polymer. If the cross-link density were to vary with depth this would have a great impact on the use of these films as, for example, biomedical coatings since such coatings have to be mechanically stable and remain strongly adhered to implant materials in challenging environments. Thus, a general goal is to tailor film and interface structure by control of processing conditions so that complicated variations in refractive index and cross-link density with depth can be designed and manufactured for various applications.

Some of the PECVD processing parameters that can be controlled to tailor interface structure may be recognized from consideration of the simplified schematic of the heart of the reactor in Figure 2. These include the reactor geometry, flow rate of reactant gases, location of precursor (monomer) feed, reactor pressure, plasma power, and plasma geometry. Here the objective is to understand how a film's structure varies with monomer feed position and plasma power so that films with highly cross-linked and uniform structures may be obtained. No broad study

Received: May 2, 2011
Accepted: August 15, 2011
Published: August 29, 2011

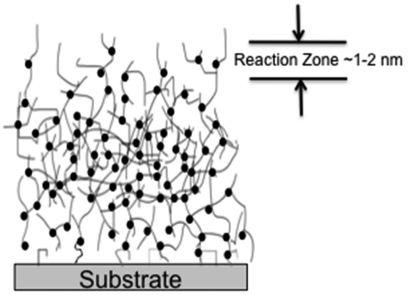

Figure 1. Schematic of a PECVD film showing its cross-linked nature, including possible variations in cross-link density with depth. Cross-link points are highlighted with dots to make them readily visible. In this particular case, cross-link densities at the air surface and substrate are lower than that in the middle of the film.

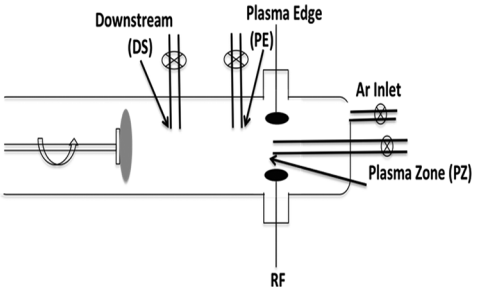

Figure 2. Schematic (not to scale) of the PECVD reactor showing three different monomer feed locations.

of depth-resolved film structure and its dependence on processing parameters has been published, although several studies targeting specific aspects of PECVD film structure or processing parameters with films of various precursors have appeared.[2,4−8]

X-ray and neutron reflectivity are exquisitely sensitive to structure in the direction perpendicular to the substrate. They can be used to resolve, to the level of several Ångstroms, the structure across an interface, including interfaces that are buried within a sample. This is unrivaled resolution among techniques able to depth profile structure in polymer films.[9] Understanding uniformity and cross-link density with depth (i.e., perpendicular to the substrate) in these films is critical in order for these films to be useful as devices for optical and photonics applications. In addition to getting information about the microstructure of air/film and internal interfaces from reflectivity measurements, simultaneous analysis of XR and NR allows one to quantify the mass density and composition at a given interface, quantities that are difficult to obtain from other experiments. In particular, complementary XR and NR measurements are ideal for characterizing the variations in chemistry near the substrate and film/air interfaces that occur because of etching and post-deposition reactions in PECVD films deposited using fluorocarbon precursors.

We are aware of three previous NR studies of PECVD film structure. Jeon and co-workers[10] probed the structure of PP- methyl methacrylate films with NR and reported that the scattering length density (SLD) (defined below) of films deposited at 60 W plasma power and reactor pressure of 0.013 Pa was uniform with depth. They further reported that NR of films swollen with good solvent vapor revealed that the films were substantially cross-linked and that the cross-link density was uniform through the film. Nelson and co-workers[11] used NR to study swelling by water of PP-allyl amine deposited at 20 W plasma power and PP-hexamethyldisiloxane homopolymer films deposited at 10 W. They reported no cross-link density variations with depth in those films. However, in a recent contribution, Peri et al.[12] showed that by adjusting the reactor pressure from 6.7 to 80 Pa the cross-link density at the substrate-interface could be varied for ultrathin plasma polymerized films of benzene and OFCB. The structure of PP-benzene films varied much more strongly with reactor pressure than did that of PP-OFCB. In this contribution, we address how feed position and plasma power impact three aspects of PP-OFCB films: the character of a transition layer next to the substrate, the uniformity of structure with depth, and the profile of cross-linking with depth.

Understanding the results requires appreciating post-deposition reactions that can occur in PP films. These reactions can significantly alter properties such as wettability and adhesion.[8,13−18] Oxygen and moisture absorption upon exposure to air have been seen in PP films deposited using fluorocarbon,[19−21] siloxane,[23] benzene,[16,17,23−25] ferrocene,[26−29] and acetylene[30] precursors. It has been further pointed out that free radicals trapped during polymer growth react with oxygen diffusing into the film to produce metastable peroxides and hydroperoxides[21,31−33] in some cases. More recently, Jiang and co-workers[29] studied oxygen absorption in PP-OFCB, PP-benzene, and PP-ferrocene films using X-ray Photoelectron Spectroscopy (XPS), electron spin resonance, and Fourier transform infrared spectroscopy. Using a downstream feed position, the authors found a significant concentration (22 at %) of oxygen at the surface of PP-ferrocene films, with far less in PP-benzene (4 at %) and PP-OFCB (0.5 at %) films. None of these precursors contain oxygen, and thus the oxygen must come from post-processing reactions. In this work, XR and NR[34−39] measurements reveal aspects of the structure next to the surface where oxygen from post-deposition reactions has been found. This helps us understand how the deposition process dictates the structure of the interface with air or with a subsequently deposited layer.

2. EXPERIMENTAL SECTION

OFCB monomer of 99 % purity (SynQuest Laboratories)[41] was used as received. Films were deposited on clean, 7.62 cm (3") diameter silicon wafers. The OFCB gas flow rate in the 10 cm diameter reactor was controlled by a mass flow controller (Sierra 902C)[41] in the range of 0.5 - 5 cm^3/min (velocities of (0.6 to 6) cm/s at the substrate face). The PECVD system has been described elsewhere.[42] Three OFCB feed locations, shown in Figure 2, were considered. The feed position in the center of the plasma zone, between the two electrodes, we denote as "plasma zone", with the abbreviation "PZ". The next feed location as one moves through the reactor, designated "plasma edge" or "PE", is at the edge of the plasma zone. Still further downstream, 10 cm from the plasma zone, is the "downstream", or "DS" position.[43] In a “feed location” series, the OFCB feed location and deposition times were varied while holding the plasma power at 30 W, the reactor pressure at 80 Pa, and the argon flow rate at 100 cm^3/min (velocity of 27.2 cm/s). In a first “power” series, plasma power and deposition time were varied for films deposited using the DS monomer feed location. In a second “power” series, plasma power and deposition time were varied for films deposited using the PZ monomer feed location. A sample name of “30PZ” indicates that the film was deposited using the plasma zone feed location and 30 W plasma power. For all films, deposition time was manipulated

in an attempt to compensate for changes in deposition rate with processing conditions to reduce the variation in thickness from film to film, but film thicknesses did vary.

X-ray photoelectron spectroscopy (XPS) measurements were done using a Surface Science Instruments[40] M-probe spectrometer equipped with a monochromatic Al K_α source with X-ray energy of 1486.6 eV. Survey scans covering binding energies between 0 and 1000 eV for a take-off angle of 30° were used to determine the composition averaged over the top 5 nm of the film. The spectrometer resolution was 1.5 eV and the analysis area was approximately 400 μm × 1000 μm. Measurements were taken at the center of each sample.

XR measurements were performed on a spectrometer mounted on a rotating anode source[43] (Rigaku,[40] 12 kW RU200) using a wavelength of 0.154 nm. The reflectivity was measured at a detector angle, with respect to the sample surface, that was equal to the incident angle, θ. The scattering vector had only a component in the z direction, q_z, which is normal to the sample surface. The spectrometer resolution in q_z was 0.01 nm^{-1}. Background scattering was measured using longitudinal diffuse scans and subtracted from the overall measured intensity to yield specular intensity.[44]

Samples were measured first in the "as-deposited" state and then variations in cross-link density with depth were probed using XR of films that were swollen with tetrahydrofuran vapor. A solvent reservoir was placed in a sealed chamber containing the sample stage and reflectivity was measured after a film had been allowed to swell for at least eight hours. Measurements of the swelling kinetics showed that the swelling did not change further after 3 h.

NR measurements were performed at the NG-7 horizontal reflectometer at the National Institute of Standards and Technology Center for Neutron Research using a wavelength of 0.475 nm and wavelength spread $(\Delta\lambda/\lambda) \approx 0.02$. The slits were adjusted to keep the footprint constant on the sample and fix the relative resolution at of $(\Delta q/q) \approx 0.04$, and the beam width was fixed at 35 mm.

The structure characteristic to which XR and NR are sensitive is scattering length density (SLD), or (b/V). For X-rays, the SLD, is related to the electron density, ρ_e, by

$$(b/V)_x = r_e\rho_e \quad (1)$$

$$\rho_e = \frac{N_A\rho_b\sum b_I}{MW} \quad (2)$$

where r_e is the classical electron radius, ρ_b is the mass density, N_A is Avogadro's number, Σb_i is total scattering length in a representative "structural unit" and is given by the sum of atomic numbers (Z_i) of the atoms in that structural unit (for wavelengths far from absorption edges), and MW is the molecular weight of that structural unit. For neutrons, the SLD can be similarly defined

$$(b/V)_n = \frac{N_A\rho_b\sum b_i}{MW} \quad (3)$$

where b_i is now the scattering length of isotope i for neutrons. The SLD profile in a sample cannot be obtained directly because of a loss of phase information, but must rather be obtained by a fitting procedure.[44,45] Parameters of a structural model supposed to capture the essential features of the sample structure are varied until agreement between the model and data is optimized. Other mathematically possible models are excluded on the basis of the requirement that they be physically reasonable given all our knowledge about the films.

RESULTS AND DISCUSSION

3.1. Variation in Structure with Monomer Feed. Key features of the way in which the films were analyzed with reflectivity can be demonstrated using the study of structure variation with feed position. Three films were deposited using a different monomer feed location for each. The deposition rate for 30 W plasma power increased as the OFCB feed location was changed from DS (0.9 nm/min) to PE (1.3 nm/min) to PZ (1.8 nm/min). Jiang and co-workers[42] did not see any changes with feed location in the chemical composition determined by XPS and Fourier Transform Infrared Spectroscopy for PP-OFCB films made under corresponding deposition conditions.

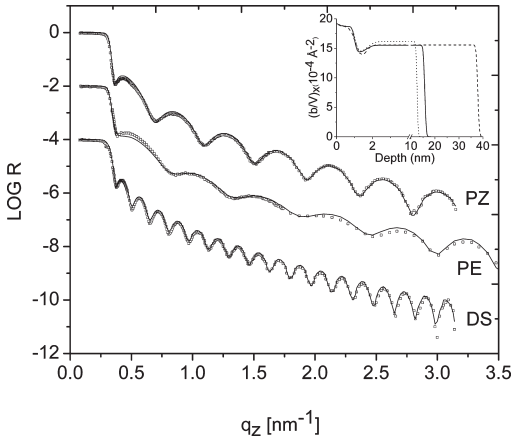

Figure 3. XR data (symbols) and best-fit curves (solid lines) for PP-OFCB films deposited at 30 W using PZ, PE, and DS feed locations, as marked. Data for PE and DS shifted along y-axis for clarity. The inset shows the SLD profiles for PZ (solid line), PE (dotted line) and DS (dashed line) films. Zero on the depth scale is taken here and elsewhere as the center of the interface between Si substrate and its oxide layer.

The XR curves for the films deposited at 30 W using PZ, PE, and DS feed locations are shown in Figure 3. These have features common to all the reflectivity curves collected and analyzed for this study. The feature that differs most notably among the reflectivity curves is spacing of the fringes which arise as a result of interference between the reflection from the polymer/air interface and the reflection from the polymer/substrate interface. The data from thicker films contain fringes with a smaller spacing. For each experimental data set a fitting procedure, described above, provides a model of the film structure expressed in the form of a one dimensional profile of SLD with depth. The model reflectivity curve, or "fit", providing the closest agreement with a given experimental data set is shown with a continuous curve. The SLD profiles corresponding to the three fits are shown in the inset of the figure. When the SLD profile is "built", two steps are used. First, an approximate "box" model is constructed by imagining the film to be a stack of ideal layers, with each layer having a uniform SLD through its depth. The thickness of each ideal layer, i, is d_i. The interface between two ideal layers is infinitely sharp. To model actual SLD variations with depth in a film these interfaces must be broadened. This is done by convoluting each infinitely sharp interface with a hyperbolic tangent profile that is parameterized using a parameter σ. Because XR and NR average over lateral variations, increasing the value of σ may represent an increasing roughness of a locally sharp interface or increasing diffuseness of an interface.[45] In the current case, σ for the polymer/air interface is probably primarily representing microroughness (i.e., ups and downs of the nominal interface), while the value of σ for an interface between two regions within the film is better thought of as representing an effective diffuseness, or breadth of the transition in structure from the one region to the

Table 1. Model Parameters for OFCB Films Deposited Using Different Feed Locations

	d (nm)[a]		b/V ($\times 10^{-4}$ nm^{-2})[b]		σ (nm)[a]	
feed	T[c]	B	T	B	T	B
DS	0.6	14.1	14.5	15.6	0.2	0.5
PE	1.0	10.7	14.9	16.1	0.2	0.4
PZ	0.6	36.3	14.7	15.5	0.2	0.5

[a] Uncertainty in thickness, d, of a layer in the model used to described the film structure is ±0.2 nm and the uncertainty in the breadth of the hyperbolic tangent function convoluted with the ideal interface at that top of that layer, σ, is 10−15%. [b] Uncertainty in SLD, b/V, is ±0.2 × 10^{-4} nm^{-2} [c] T = transition layer, B = bulk layer .

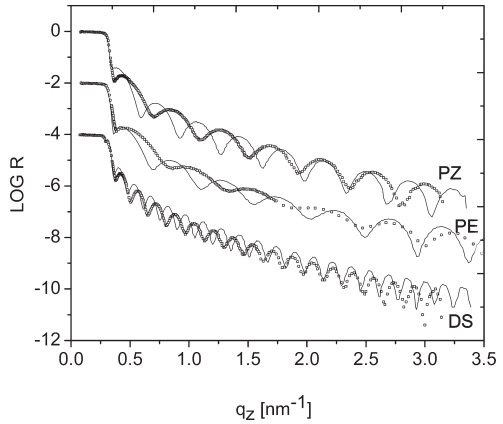

Figure 4. XR data for as-deposited (open squares) and after swelling (solid lines) for the PP-OFCB samples deposited using the PZ, PE, and DS feed locations and plasma power of 30 W. The curves for PE and DS feed locations have been shifted along the y-axis for clarity.

next. The very small values of σ seen for the interfaces with native oxide on the silicon substrate are consistent with the well-established fact[9−12] that such substrates are nearly atomically smooth.

For modeling the XR and NR data from the PP-OFCB films for all process conditions considered here, it was necessary to include in the structural model a thin transition layer between the oxide and the layer describing the majority of the polymer film as first observed by Kim et al.[9] The fact that the transition in structure occurs over such a small depth, ca. 1 nm, suggests that only a few layers of organic fragments deposited at the surface are necessary to substantially screen the influence of the oxide as far as surface chemical reactivity is concerned.

Several similarities among the structures of the films are observed. First, the majority of the polymer layer, or "bulk", can be described using a uniform SLD. Secondly, the interface between polymer and air is very smooth, regardless of feed location, with a value of σ (≈ 0.5 nm) only slightly larger than that of the underlying SiO_x (≈ 0.3 nm). Thirdly, the mass densities of the films are the same within our experimental uncertainties. For understanding the structure of the film it is most instructive to study the SLD profiles themselves. However, for archiving or reconstructing the profiles one used the parameters of the "box" model of ideal layers and the breadths of the convolutions functions used to smear out the interfaces. For comparison, these parameters of the model structure

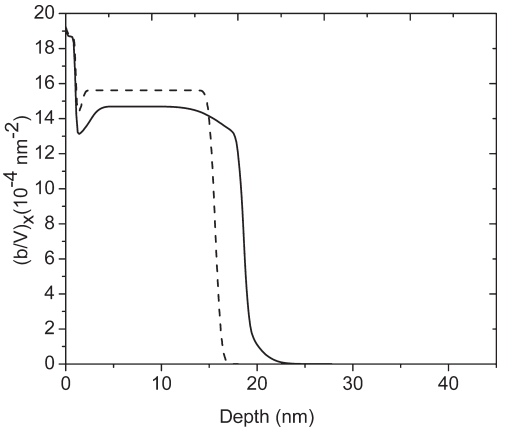

Figure 5. X-ray SLD profiles for the as-deposited (dashed line) and swollen (solid line) sample deposited using the PZ feed location and 30 W power.

corresponding to best fit for each sample are given in Table 1. In each case, a good fit with a value for the normalized sum of squared errors, χ^2, of less than 1.3 was obtained. No striking differences with monomer feed location were observed at 30 W, but differences observed at higher power are discussed below.

3.2. Variation in Structure with Monomer Feed: Cross-link Density Comparisons. Comparison of XR data before and after the exposure to tetrahydrofuran vapor for films deposited at 30 W shows that each swells with exposure to solvent, but that the interfaces are not appreciably roughened or broadened. These data are shown in Figure 4. The reason for swelling with solvent is to probe how the cross-link density varies with depth. The decrease in fringe spacing with exposure to solvent indicates that each film swelled. The fact that the fringes in the curves for swollen films persist to the highest values of q for which measurements were made signifies that the interfaces do not broaden or roughen appreciably with swelling. To quantify how each film swells, we compare SLD profiles before and after swelling in Figure 5 (fits and SLD profiles for samples deposited using PE and DS monomer feed are shown in supplemental material Figures S1, S2, and S3).

For all three feed locations, solvent swells the transition region, bulk, and the portion of the film next to the air interface. Because the solvent SLD is less than that of the polymer, the larger reduction in SLD near the air interface shows that a higher concentration of solvent is taken up there. The top 1.5 nm to 3.0 nm (thickness before swelling) of the film is more loosely cross-linked than is the bulk of the film. We conjecture that the loosely cross-linked layer at the air-interface develops as a result of the way in which the deposition occurs. When the deposition is progressing, reactive fragments landing on the film may react at the topmost surface or diffuse a short distance into the film, reacting with parts of the as yet incomplete network near the surface. When the deposition is stopped, a gradient in cross-link density in the first 1.5 nm to 3.0 nm of the film is fixed. This cross-link density gradient is not apparent in the XR SLD profile when the film is dry, but upon swelling it becomes apparent. Thus, the swelling measurements provide evidence for a finite depth of a reactive zone at the interface for all feed locations.

The reduced cross-link density in the transition region can be attributed to reactions between the oxide layer and the incoming fluorine species. Fluorine-rich fragments, being very electronegative,

Table 2. Overall Degrees of Swelling for Films Deposited with Different Feed Locations

feed	total film thickness dry (nm) ±.2 nm	total film thickness swollen (nm) ±.2 nm	% swelling
PE	13.5	16.5	22
PZ	16.0	19.0	18
DS	39.5	42.5	8

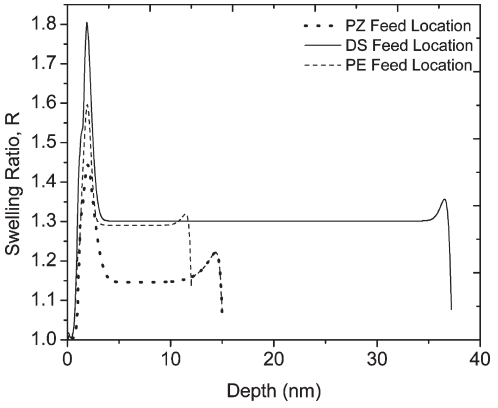

Figure 6. Swelling ratio with dry depth for samples deposited at 30 W plasma power, 80 Pa pressure, and PZ feed location (dotted line), PE feed location (dashed line), and DS feed location (solid line).

are repelled from the negatively charged oxide, thus forming only a few covalent connections between the oxide and the transition layer.[9] The presence of a low cross-link density next to the oxide is consistent for all PP-OFCB films regardless of monomer feed location and plasma processing power as discussed below. This information about precisely where in the films the swelling occurs allows us to understand the values of overall swelling, shown in Table 2.

Because the degree of swelling is much larger in the thin regions next to the substrate and air than elsewhere in the films, the overall degree of swelling is a strong function of total film thickness. Thinner films, for which these interfacial regions constitute a larger fraction of total film volume, have larger overall degrees of swelling. Thus, dimensional stability of these films in the presence of solvents is of greatest concern for the thinnest films.

To find variations in cross-link density with depth we calculate swelling ratio (R) as a function of depth as explained in the Supporting Information. Figure 6 shows the variation in *R* with dry depth for samples deposited using PZ, PE, and DS monomer feed locations. For all three cases, a large peak in swelling ratio at the transition region and a smaller peak at the air-interface indicate regions which are relatively loosely cross-linked as compared to the "bulk" of the film. The cross-linking in the transition region appears to decrease as the feed location is moved from PZ to PE to DS, while the cross-linking in the "bulk" is highest for the PZ location, but about the same for PE and DS samples. Samples deposited using the DS and PE feed locations have "surface regions" thinner than that in the sample deposited using the PZ feed location. We note that the deposition rate is highest for the PZ case and that the most energetic species are created for the PZ feed.

3.3. Variation in Structure with Processing Power. Consideration of NR data from films deposited at different powers shows the capability of the technique to reveal variations in composition depth profile and variations in interface roughness.

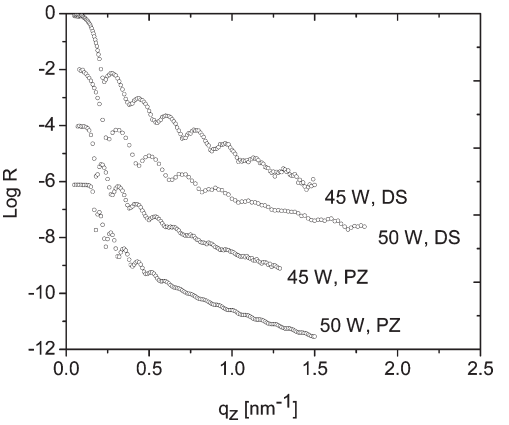

Figure 7. NR data for films deposited using DS feed location and processing power of 45 and 50 W and using PZ feed location and processing power of 45 and 50 W. The data for 50 W, DS and 45 and 50 W, PZ samples have been shifted along the *y*-axis for clarity.

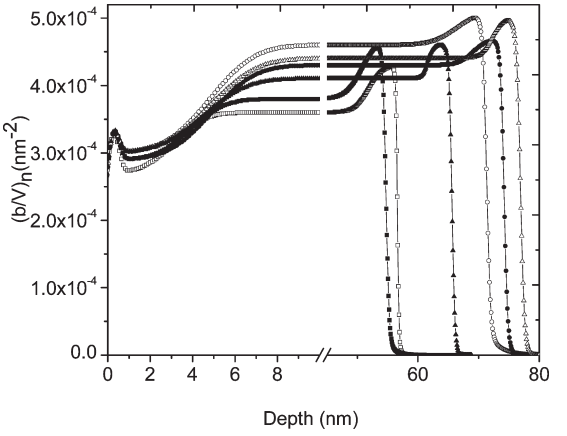

Figure 8. Neutron scattering length density profile for samples deposited at 40 W (open squares), 45 W (filled squares), 50 W (open circles), 55 W (filled circles), 60 W (open triangles), and 65 W (filled triangles) using the PZ feed location.

The most notable differences are in the structures next to the air surface between the films deposited at plasma powers below 40 W and above 40 W. (Data and fits for all powers in the Supporting Information, Figure S4). In the NR data for the dry films deposited at powers above 40 W, shown in Figure 7, the fringe amplitude dies very quickly for the samples deposited using the PZ location, indicating that there is at least one broad interface present in each of these samples. The neutron SLD profiles for the samples deposited using the PZ location are shown in Figure 8 (Data from DS samples discussed below, with the corresponding film structure model parameters in the Supporting Information, Table S1). The transition region next to the oxide seen in the SLD model for the NR data is twice as broad as the transition region reported by Kim and co-workers[9] for films deposited using the DS feed location and 30 W power. We conjecture that for samples deposited at 40−65 W plasma power using the PZ feed location, the reactive fragments etch the silicon oxide interface significantly, thus broadening the transition region.

Analysis of XR data (see the Supporting Information, Figure S5 and S6 and Table S2) from the same samples provides

complementary information. The transition layer and "surface layer" seen with NR do not manifest themselves in the XR SLD profiles in the same way as in the NR SLD profiles. Although the existence of a transition region is apparent from the SLD profiles derived from both NR and XR, the NR SLD profiles suggest a transition region about four times as broad as that evidenced in the XR SLD profiles. The minimum X-ray SLD and minimum neutron SLD in the transition region do not change with plasma power in a systematic way. This suggests that we may be able to use the complementary data from XR and NR to infer a value of mass density in that part of the film if we have some composition information. Standaert and co-workers,[46] Cadinaud and co-workers,[47] and Easwarakhanthan and co-workers[48] have studied, with XPS and Fourier transform infrared spectroscopy, the different species that result from the etching of a SiO_2 surface with fluorocarbons. They report etch products including SiF_y, $Si_xC_yF_z$, and mixtures of SiOF, SiOC, and COF. The relative compositions of these different species vary with plasma power. Using values of the XR and NR SLDs, the mass density and composition in the transition region may be estimated. These are difficult to obtain otherwise. The key is that the dependences of the two SLDs on composition and mass density must be satisfied simultaneously. Because the ratios of scattering lengths of C, F, and Si are quite different for XR and NR, if one insists that the composition of each of these elements be nonzero, only a narrow range of empirical formulae are feasible. Once the empirical formula is defined, the mass density in the transition region can be calculated. Simultaneously satisfying the XR and NR SLD values, a value of 1.7 ± 0.06 g/cm^3 is found for the mass density and an empirical formula $C_2F_{1.6}Si_{1.6}$ found for the composition. This is consistent with our expectation that near the oxide, CF radicals would be favored over the more highly electronegative CF_2 and CF_3 radicals. It was impossible to obtain any physically reasonable results for mass density and composition when including nonzero values of oxygen content.

A second difference between the structure models suggested by the NR and XR data for this power series of samples with PZ feed concerns the "surface layer". The XR data could be fit without using a "surface" layer in the film structure model, whereas this feature was essential for fitting the NR data. To explain this seeming discrepancy, one must consider how the SLD depends on the structure for these two types of radiation. The neutron scattering lengths for fluorine and oxygen are 14% lower than the b_i for carbon, whereas the X-ray scattering length for fluorine is higher than that of either oxygen or carbon. From XPS we have elemental compositions of C, F, and O from that portion of the sample probed under standard conditions, which is about the first 5 nm of the film. This corresponds roughly to the thickness of the surface layer seen in the NR models. We anticipate that more oxygen and carbon and less fluorine at the surface could explain the high $(b/V)_n$ seen in NR and a small change in $(b/V)_x$ from XR.

When the feed location is moved downstream from PZ to DS, the deposition rate drops markedly and the way in which deposition varies with power is altered (shown in the Supporting Information, Figure S7). The deposition rate increases linearly with increasing power for the PZ samples. For the DS feed location, the deposition rate first increases with power, reaches a maximum and then decreases as the power is further increased. We conjecture that in the PZ feed region, many high-energy species including ions, electrons, radicals, and excited species are available for OFCB dissociation, whereas in the DS feed regio,

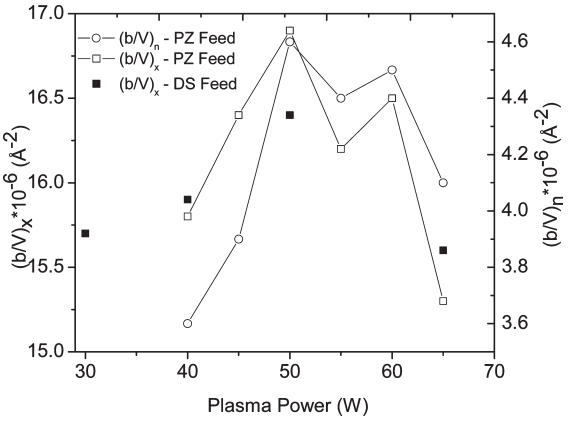

Figure 9. Variation in XR and NR SLD with plasma power for PZ and DS feed. The uncertainties in XR and NR SLD's is $\pm 0.1 \times 10^{-4}$ nm^{-2}. Lines are guides to the eye.

only metastable species are present. We anticipate that a maximum in deposition rate would be observed for depositions using the PZ feed also if sufficiently high powers were investigated. Several studies[49,50] have reported such a maximum in deposition rate with power for fluorocarbon and ethylene precursors.

We also studied how film structure varies with plasma power for the case of the DS feed location (NR curves, SLD profiles and model fit parameters are shown in the Supporting Information, Figures S8 and S9 and Table S3). Two similarities are found in the way structure varies with power for the DS and PZ feed locations. First, a critical power (40 W) is observed above which a "surface" layer is present that has a composition different from the "bulk" composition (Figure 8). We suggest that the "surface" layer is the result of two causes, one connected with the deposition process itself. The second process dictating the character of the surface layer is reaction between the residual radicals and species diffusing into the film when the film is exposed to ambient. That the layer is present at all is not peculiar to specific chemistry, but rather is a general feature of the deposition mechanism. At deposition powers used here (which are higher than that considered in our earlier work[9]), a high concentration of unreacted free radicals is left in the film and these radicals are capable of oxidation.[51,52]

The second similarity between the variation with power seen for the DS and PZ feed positions is that the SLD reaches a maximum at 50 W and decreases as the power is further increased, as shown in Figure 9. We conjecture that ion bombardment, which increases with increasing power, initially leads to denser films, but further increase in power leads to increased sputtering of the growing film, which decreases the film density. In fact, our comparisons using apparent plasma power are only approximate at higher powers, because at 65 W the aluminum electrode begins to be sputtered, which means that the actual energy coupled into the plasma is less than the apparent energy input.

4. Variation in Cross-link Density with Processing Power (DS Feed Location). For a film deposited with downstream feed, cross-link density in the film increases with plasma power. This is seen from comparisons of XR data taken before and after swelling (SLD profiles for 30 W given above in Figure 5, other curves and fits in the Supporting Information, Figures S10 and S11). The dry sample thickness is not changed by one cycle of swelling and drying for samples deposited at 40 and 50 W. How the cross-link

density varies with depth for the different deposition powers may be deduced once again from plots of SLD profiles before and after swelling (see the Supporting Information, Figures S12 and S13) and calculation of the swelling ratio as a function of depth (see the Supporting Informatiom, Figure S14).

For samples deposited at 40 and 50 W, lower cross-link densities are present at the air and substrate interface. The variation in swelling ratio with depth is similar in character to that for samples deposited at 30 W using the three feed locations (Figure 6). The origin of the region of different structure next to the substrate has been considered in an earlier publication.[9] The presence, specifically, of a lower cross-link density at the substrate was first reported in our recent study of ultrathin films,[12] but the generality of this phenomenon becomes apparent only with the extensive data set considered here. A region of different structure at the air interface is seen at all plasma powers considered here and its width is similar for different plasma powers. Therefore, we conjecture that its presence provides an important hint regarding how the film is deposited and how layer/layer interfaces are formed in the case that the deposition of one layer is followed by deposition of a layer using a different precursor, as was done in ref 9.

We conjecture that the low cross-link density region at the air surface at powers of 40 and 50 W reflects the fact that while the film is being deposited, reaction of incoming reactive species with the material already on the surface occurs not only on the topmost surface, but down to a depth of about 1.0 nm to 1.5 nm (see "reaction zone", Figure 1). This is a depth to which incoming reactive species are able to diffuse before reacting. In the case of the 30 W sample, material somewhat below the surface of the film at a given point in the deposition is still not as tightly cross-linked as it could be, but as further material is deposited on top of the film, reactive sites farther than ca. 3.0 nm from the surface become inaccessible to incoming reactive species. The depth of this surface reaction zone is a key feature of the deposition that determines the width of interfaces formed when a layer of one precursor is deposited atop a layer from another precursor.

The variation in overall degree of film swelling by vapor with film thickness for films deposited at various powers is modest in all the cases (shown in Figure S15 and the swelling parameters in Table S4 in the Supporting Information). However, because the swelling occurs disproportionately next to the substrate and next to the air, the overall degree of swelling depends not only on plasma power, but also on film thickness. For the thicknesses studied here, the larger swelling of the interfacial regions dominates the overall behavior, as seen also for the series at 30 W using different feed locations (section 3.2).

For the sample deposited at 65 W, analysis of the reflectivity from the swollen state, plotted in Figure S16 in the Supporting Information, reveals an additional aspect of the change in deposition with power. That sample is altered by the swelling process, and SLD profiles are shown in Figure 10 for three states of the sample.

For the 65 W sample, measuring the swelling reveals that fragmentation of the film structure occurs simultaneously with deposition and fragments of high fluorine content can move to the surface when the film is swollen. After swelling, the reflectivity at higher values of q_z increases, which indicates that there is a surface region in which the SLD is significantly higher than that

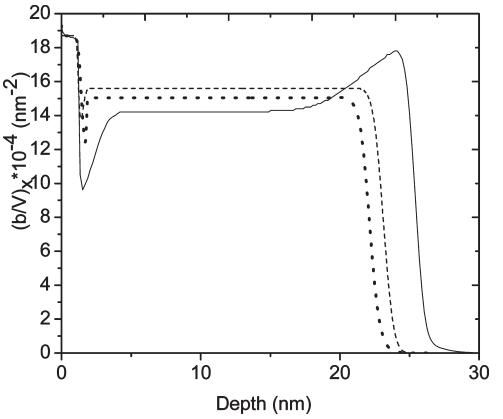

Figure 10. X-ray SLD profiles for the PP-OFCB sample deposited using DS feed and 65 W power: as-deposited sample (dashed line), swollen with vapor the first time (solid line), dry again (dotted line).

in the center of the film and higher than the SLD of the dry film. Because the solvent $(b/V)_x$ (= 9.08×10^{-4} nm^{-2}) is significantly lower than that of the fluorine-containing polymer, the only way to explain the increase in SLD near the surface is to postulate that material with a degree of fluorination higher than the average in the film has migrated to the surface upon swelling. The preferential segregation of low energy species to a film surface to minimize overall free energy is well-known,[53,54] but necessitates a mobility of species in the film that is inconsistent with a model in which all the organic material is in a cross-linked network. The sample deposited at 65 W, while more highly cross-linked, also contains loose fragments of composition C_uF_v with $v/u > 2$ and u of a value such that the fragment is not removed from the film under the low pressure in the reactor during the deposition, but can move when the film is swollen. We conjecture that these fragments are formed by sputtering of the polymer that occurs concurrently with deposition. When the sample was measured with XR again after drying to remove solvent, the dry film thickness had decreased by about 6%. The SLD profile for the dried sample shows no evidence of surface segregation of higher $(b/V)_x$ material, suggesting that material was removed with the evaporation of the solvent. The lower value of SLD in the "bulk" of the film after drying is consistent with this contention that a small fraction of more highly fluorinated material has been extracted. None of the samples deposited at lower powers lost thickness after being swollen with vapor and dried. Because swelling for the 65 W sample was accompanied by a redistribution of fluorinated material, it is not reasonable to attempt a quantification of the variation in swelling ratio with depth. The dip in SLD near the substrate in the swollen 65 W sample could be consistent with a greater degree of swelling there. However, it is also conceivable that the movement of more highly fluorinated fragments to the outer surface of the sample by the swelling could be responsible, in part, for the precise depth of the dip. The minimum of the dip ($b/V \approx 10 \times 10^{-4}$ nm^{-2}) is lower than for any of the films deposited at lower powers.

3.8. Implications of Reaction Zone. The importance of a reaction zone next to the surface is manifested clearly for the case of a thin bilayer film made from deuterated-benzene (dB) and OFCB precursors. The sample was made by first depositing a 3.5 nm thick PP-dB layer on the substrate and then depositing a much thicker layer of PP-OFCB without taking the sample from the reactor, which remained under vacuum. The PP-dB was

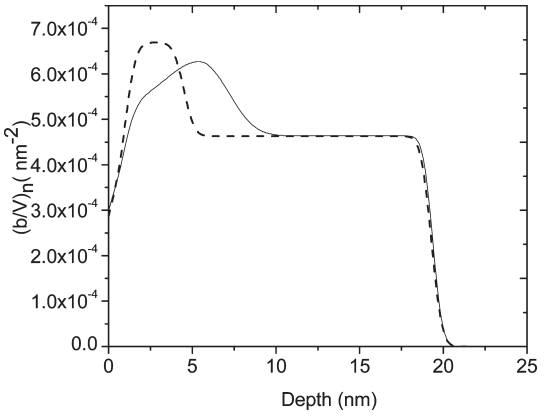

Figure 11. Neutron SLD profile for bilayer sample deposited at 20 W using the DS feed location for dB and the PZ feed location for OFCB. The dashed curve is a hypothetical profile that would be expected if the bottom layer in the bilayer were identical to a thin homopolymer PP-dB film and the layer/layer interface were as sharp as the interfaces formed with air. The solid curve is the experimentally determined profile.

deposited using the DS feed position and PP-OFCB using the PZ position, both with a power of 20 W. The NR data and fit are shown in the Supporting Information (Figure S17) and the SLD profile corresponding to the fit is shown in Figure 11. The dashed line shows the composition profile we should expect if the structure of the dB layer were similar to that seen in a thicker, single layer PP-dB film or in bilayers studied previously.[9] In those cases, the SLD in the PP-dB layer reached a value consistent with that of PP-dB homopolymer films.[9] The SLD found here next to the substrate is lower than would be expected for the same position in a thicker PP-dB layer. It could be that there is a region of low mass density next to the substrate with the fragments incorporated there being only dB fragments. However, this would be inconsistent with SLD profiles obtained for single layer PP-dB films and is very unlikely. It is more plausible that OFCB monomer fragments were able to diffuse through the PP-dB layer, the total thickness of which was comparable to the depth of the reaction zone postulated above. If the entire PP-dB layer had the character of the "incomplete" structure in the reaction zone, OFCB fragments could penetrate all the way to the substrate surface and at the substrate interface there would be a copolymeric structure containing both dB and OFCB fragments having a value of SLD between those of PP-OFCB and PP-dB. This is consistent with what we see. Kim et al.[9] reported an average interface width of 1.9−2.0 nm, reported as σ, between a PP-dB lower layer and PP-OFCB upper layer in bilayer and multilayer films. They conjectured that the layer/layer interface widths they saw were larger than the film/air interface widths they saw because of the local chemistry that occurs when interfaces are formed. However, on the basis of the evidence gathered in this work, we suggest that the layer/layer interface width is larger than the layer/air interface width due to the manner in which the material in the second layer "fills in" the reaction zone left at the top of the first layer.

4. CONCLUSIONS

XR and NR measurements provide a wealth of information about variations in the structures of PECVD films with changes in feed position and plasma power. For the plasma powers and feed positions studied here, a region of different chemical composition and lower cross-link density is always observed at the substrate interface. When the plasma power exceeds 40 W, a surface layer of lower cross-link density of about 3 nm thickness appears at the air interface. While there are several similarities in the film structure for depositions done with various feed positions, details vary. When the feed position is pushed into the plasma zone, the cross-linking in the center of the films is highest, the surface layer is somewhat thicker, and the region of transition in structure at the substrate is thicker than when the feed is farther from the plasma. Also, for the PZ feed, the film scattering length density goes through a maximum with power in the range studied. At the highest power, 65 W, whereas the cross-linking is highest, loose fragments with fluorine content higher than the average are also present and can be removed by swelling with solvent and drying.

The gradient in cross-link density near the air interface that is left when deposition of a layer is halted gives evidence that deposition occurs not only at the outer surface of a film, but rather over a reaction zone of finite depth. The depth of this reaction zone is a key factor in determining the layer/layer interface widths in multilayer PP-films and therefore has implications for potential uses of such films. Because the reaction zone is on the order of 1−3 nm thick, layer/layer interfaces can be created that are very sharp by the standards of optical applications, which makes them attractive. At the same time, the structural interpenetration that results from deposition into the reaction zone of the preceding layer is large enough to provide good adhesion between the layers if the reactive fragments of second layer react well with the existing structure of the first layer. How well this "copolymerization" occurs at the interfaces in multilayers could be probed with swelling measurements. The existence of the reaction zone also suggests possibilities for post deposition chemistry for the purposes of tailoring surface properties of the films. Because it is clear that radicals in the reaction zone are available for reaction upon exposure to the ambient, one could choose instead to, for example, expose the film to some gas other than oxygen before opening the reactor. This could be used to alter the hydrophobicity of the surface or other properties.

■ ASSOCIATED CONTENT

Supporting Information. Data and fits, SLD profiles, and tables containing best fit parameters and a description of the swelling ratio (R) with depth calculation are included. This information is available free of charge via the Internet at http://pubs.acs.org/.

■ AUTHOR INFORMATION

Corresponding Author
*E-mail: mfoster@uakron.edu.

■ ACKNOWLEDGMENT

This research was funded by the Collaborative Center for Polymer Photonics (49620-02-1-0428) which is co-funded by the Air Force Office of Scientific Research, Air Force Research Laboratory, and The University of Akron. We acknowledge support of the National Institute of Standards and Technology, U.S. Department of Commerce, in providing the neutron research facilities used in this work.

REFERENCES

(1) Beck, A. J.; Jones, F. R.; Short, R. D. *Polymer* **1996**, *37*, 5537–5539.
(2) Hirotsu, T.; Tagaki, C.; Partridge, A. *Plasmas Polym.* **2002**, *7*, 353–366.
(3) Grant, J. T.; Jiang, H.; Tullis, S.; Johnson, W. E.; Eyink, K.; Fleitz, P.; Bunning, T. J. *Vacuum* **2005**, *80*, 12–17.
(4) Yin, Y.; Wise, S. G.; Nosworthy, N. J.; Waterhouse, A.; Bax, D. V.; Youssef, H.; Byrom, M. J.; Bilek, M. M.; McKenzie, D. R.; Weiss, A. S.; Ng, M. K. *Biomaterials* **2009**, *30*, 1675–1681.
(5) Jiang, H.; O'Neill, K.; Grant, J. T.; Tullis, S.; Johnson, W. E.; Eyink, K.; Fleitz, P.; Bunning, T. J. *Chem. Mater.* **2004**, *16*, 1292–1297.
(6) Benitez, F.; Martinez, E.; Galan, M.; Serrat, J.; Esteve, J. *Surf. Coat. Technol.* **2000**, *125*, 383–387.
(7) Dilsiz, N.; Akovali, G. *Polymer* **1996**, *37*, 333–342.
(8) Yasuda, H. *Plasma Polymerization*; Academic Press: Orlando, FL, 1985.
(9) Kim, H.; Foster, M. D.; Jiang, H.; Tullis, S.; Bunning, T. J.; Majkrzak, C. F. *Polymer* **2004**, *45*, 3175–3184.
(10) Jeon, H. S.; Wyatt, H. D.; Weinkauf, D. H. *J. Polym, Sci., Part B: Polym. Phys.* **2004**, *42*, 2522–2530.
(11) Nelson, A.; Muir, B. W.; Oldham, J.; Fong, C.; McLean, K. M.; Hartley, P. G.; Oseth, S. K.; James, M. *Langmuir* **2006**, *22*, 453–458.
(12) Peri, S. R.; Habersburger, B. H.; Akgun, B.; Jiang, H.; Enlow, J.; Bunning, T. J.; Majkrzak, C. F.; Foster, M. D. *Polymer* **2010**, *51*, 4390–4397.
(13) Engleman, R. A.; Yasuda, H. *Polym. Mater. Sci. Engr.* **1990**, *62*, 19–25.
(14) Gazicki, M.; Yasuda, H. *Plasma Chem. Plasma Process.* **1983**, *3*, 279–288.
(15) Morosoff, N.; Haque, R.; Clymer, S. D.; Crumbliss, A. L. *J. Vac. Sci. Technol., A* **1985**, *3*, 2098–2101.
(16) Gengenbach, T. R.; Chatelier, R. C.; Griesser, H. J. *Surf. Interface Anal.* **1996**, *24*, 271–281.
(17) Gengenbach, T. R.; Chatelier, R. C.; Griesser, H. J. *Surf. Interface Anal.* **1996**, *24*, 611–619.
(18) Kuzuya, M.; Kondo, S. I.; Sugito, M.; Yamashiro, T. *Macromolecules* **1998**, *31*, 3230–3234.
(19) Hetzler, U.; Kay, E. *J. Appl. Phys.* **1978**, *49*, 5617–5623.
(20) Friedrich, M.; Hinze, D.; Ebert, W. *Thin Solid Films* **1984**, *112*, 61–69.
(21) Momose, Y.; Ohaku, T.; Chuma, H.; Okazaki, S.; Saruta, T.; Masui, M.; Takeuchi, M. *J. Appl. Polym. Sci.* **1990**, *46*, 153–172.
(22) Wrobel, A. M. *J. Macromol. Sci., Part A: Pure Appl. Chem.* **1985**, *A22*, 1089–1100.
(23) Kuzuya, M.; Noguchi, H.; Kondo, S.-i.; Noda, N. *J. Polym. Sci., Part A: Polym. Chem.* **1991**, *29*, 1–15.
(24) Kuzuya, M.; Morisaki, K.; Niwa, J.; Yamauchi, Y.; Xu, K. *J. Phys. Chem.* **1994**, *98*, 11031–11036.
(25) Gengenbach, T. R.; Greisser, H. J. *Polymer* **1999**, *40*, 5079–5088.
(26) Ob"edkov, A. M.; Domrachev, G. A.; Khorshev, S. Ya.; Suvorova, O. N.; Vasilevskaya, I. L. *Russ. J. Gen. Chem.* **2003**, *73*, 331–333.
(27) Han, L. M.; Rajeshwar, K.; Timmons, R. B. *Langmuir* **1997**, *13*, 5941–5950.
(28) Enlow, J. O.; Jiang, H.; Grant, J. T.; Eyink, K.; Su, W.; Bunning, T. J. *Polymer* **2008**, *49*, 4042–4045.
(29) Jiang, H.; Grant, J. T.; Enlow, J.; Su, W.; Bunning, T. J. *J. Mater. Chem.* **2009**, *19*, 2234–2239.
(30) Yasuda, H.; Marsh, H. C.; Bumgarner, M. O.; Morosoff, N. *J. Appl. Polym. Sci.* **1975**, *19*, 2845–2858.
(31) Wang, D.; Chen, J. *J. Appl. Polym. Sci.* **1991**, *42*, 233–252.
(32) Chen, J. *J. Appl. Polym. Sci.* **1991**, *42*, 2035–2047.
(33) Yasuda, H. *J. Macromol. Sci.—Chem.* **1976**, *A10*, 383–420.
(34) Blasie, J. K.; Zheng, S.; Strzalka, J. *Phys. Rev. B: Condens. Matter* **2003**, *22*, 224201–224208.
(35) Lagomarsino, S.; Di Fonzo, S.; Jark, W.; Muller, B.; Cedola, A.; Pelka, G. *Mater. Res. Soc. Symp. Proc.* **1995**, 381–389.
(36) Benattar, J. J.; Schalchli, A. *Phys. Scr.* **1994**, *50*, 188–194.
(37) Geer, R.; Qadri, S.; Shashidhar, R.; Thibodeaux, A. F.; Duran, R. S. *Liq. Cryst.* **1994**, *16*, 869–875.
(38) Ziegler, E.; Ferrero, C.; Lamy, F.; Chapron, C.; Morawe, Ch. *Adv. X-Ray Anal.* **2002**, *45*, 345–371.
(39) Zymierska, D.; Sobczak, E.; Godwod, K.; Miotkowska, S. *J. Appl. Crystallogr.* **1998**, *17*, 394–397.
(40) Commercial materials, instruments, and equipment are identified in this paper in order to specify the experimental procedure as completely as possible. In no case does such identification imply a recommendation or endorsement by the National Institute of Standards and Technology nor does it imply that the materials, instruments, or equipment identified are necessarily best available for the purpose.
(41) Jiang, H.; O'Neill, K.; Grant, J. T.; Tullis, S.; Eyink, K.; Johnson, W. E.; Fleitz, P.; Bunning, T. J. *Chem. Mater.* **2004**, *16*, 1292–1297.
(42) Jiang, H.; Grant, J. T.; Tullis, S.; Eyink, K.; Enlow, J.; Bunning, T. J. *Polymer* **2005**, *46*, 8178–8184.
(43) Vierheller, T. R. *PhD Thesis*. The University of Akron, Akron, OH, 1994.
(44) Sheller, N. B.; Petrash, S.; Foster, M. D.; Tsukruk, V. V. *Langmuir* **1998**, *16*, 4535–4544.
(45) Foster, M. D. *Crit. Rev. Anal. Chem.* **1993**, *24*, 179–241.
(46) Standaert, E. T.; Hedlund, C.; Joseph, E. A.; Oehrlein, G. S.; Dalton, T. J. *J. Vac. Sci. Technol.* **2004**, *22*, 53–60.
(47) Cardinaud, Ch.; Turban, G. *Appl. Surf. Sci.* **1990**, *45*, 109–120.
(48) Easwarakhanthan, E.; Beyssen, D.; Le Brizoual, L.; Bougdira, J. *J. Vac. Sci. Technol.* **2006**, *24*, 1036–1043.
(49) Nakajima, K.; Bell, A.; Shen, M. *J. Appl. Polym. Sci.* **1979**, *23*, 2627–2637.
(50) Kurosawa, S.; Choi, B. G.; Park, J. W.; Aizawa, H.; Shim, K. B.; Yamamoto, K. *Thin Solid Films* **2006**, *506*, 176–179.
(51) Horie, M. *J. Vac. Sci. Technol.* **1995**, *13*, 2490–2497.
(52) Yasuda, H.; Bumgarner, M. O.; Marsh, H.C.; Morosoff, N. *J. Polym. Sci., Part A: Polym. Chem.* **1976**, *14*, 195–224.
(53) Balaji, R.; Koberstein, J. T.; Bhatia, Q. S. *Polym. Mater. Sci. Eng.* **1991**, *62*, 876–880.
(54) Elman, J. F.; Johs, B. D.; Long, T. E.; Koberstein, J. T. *Macromolecules* **1994**, *27*, 5341–5349.